PAPER

Permeation through graphene ripples

To cite this article: Tao Liang *et al* 2017 *2D Mater.* **4** 025010

2D Materials

PAPER

Permeation through graphene ripples

RECEIVED
16 November 2016

REVISED
21 December 2016

ACCEPTED FOR PUBLICATION
16 January 2017

PUBLISHED
1 February 2017

Tao Liang[1,6], Guangyu He[2,6], Xu Wu[3,6], Jindong Ren[3], Hongxuan Guo[4], Yuhan Kong[1], Hideo Iwai[5], Daisuke Fujita[4], Hongjun Gao[3], Haiming Guo[3], Yingchun Liu[2] and Mingsheng Xu[1]

[1] College of Information Science & Electronic Engineering, State Key Laboratory of Silicon Materials, Zhejiang University, Hangzhou 310027, People's Republic of China
[2] Department of Chemistry, Zhejiang University, Hangzhou 310027, People's Republic of China
[3] Beijing National Laboratory of Condensed Matter Physics, Institute of Physics, Chinese Academy of Sciences, Beijing 100190, People's Republic of China
[4] Nano Characterization Unit, National Institute for Materials Science, Sengen 1-2-1, Tsukuba, Ibaraki 305-0047, Japan
[5] Surface & Microbeam Analysis, Materials Analysis Station, National Institute for Materials Science, Sengen 1-2-1, Tsukuba, Ibaraki 305-0047, Japan
[6] Tao Liang, Guangyu He and Xu Wu contributed equally to this work.

E-mail: msxu@zju.edu.cn, liuyingch@zju.edu.cn and hmguo@iphy.ac.cn

Keywords: grapheme, ripples, permeation, DFT calculations

Supplementary material for this article is available online

Abstract

Real graphene sheets show limited anti-permeation performance deviating from the ideally flat honeycomb carbon lattice that is impermeable to gases. Ripples in graphene are prevalent and they could significantly influence carrier transport. However, little attention has been paid to the role of ripples in the permeation properties of graphene. Here, we report that gases can permeate through graphene ripples at room temperature. The feasibility of gas permeation through graphene ripples is determined by detecting the initial oxidation sites of Cu surface covered with isolated graphene domain. Nudged elastic band (NEB) calculations demonstrate that the oxygen atom permeation occurs via the formation of C–O–C bond, in which process the energy barrier through the rippled graphene lattice is much smaller than that through a flat graphene lattice, rendering permeation through ripples more favorable. Combining with the recent advances in atoms intercalation between graphene and metal substrate for transfer-free and electrically insulated graphene, this discovery provides new perspectives regarding graphene's limited anti-permeation performance and evokes for rational design of graphene-based encapsulation for barrier and selective gas separation applications through ripple engineering.

1. Introduction

A perfect graphene sheet is impermeable to all atoms and molecules [1–4], contrary to protons [5, 6], under ambient conditions. This feature is mainly attributed to its honeycomb lattice and the electron density of its aromatic rings, which is sufficiently strong to repel atoms and molecules trying to pass through the lattice. Ripples exist inevitably in graphene [7–12] and significantly influence carrier transport [8, 13–16]. Intercalation of different atoms at the interface between graphene and its metal substrate has been widely observed [17–19], however, mechanisms of the intercalation remain unclear. Alternatively, the opening of small holes [20, 21] in graphene sheets enables the selective permeation of small molecules. The formation of ripples in graphene can be due to the supporting substrate [8] and the thermal fluctuation of the graphene itself [7, 22]. In this system, ripples in graphene stand out as out-of-plane deviations that help to stabilize graphene [7–10]; ripples can also decrease in-plane elastic moduli of graphene, leading to destabilization [11, 12]. The lattice deformations induced by ripples can effectively generate electric and magnetic fields acting on the propagating Dirac fermions, thereby strongly modifying graphene's electronic properties and transport behavior [8, 13–16, 23, 24]. A previously theoretical study has shown that such ripples could also influence the chemical reactivity, binding energy and adsorption barrier of graphene [25] by changing the atomic and electronic structures of the corrugated carbon scaffold. An experimental study further demonstrated an enhanced chemical reactivity at the locally curved surface of graphene [26]. However, experimentally investigating the influence of graphene ripples with deformed lattices on the permeation

of chemical species through graphene is extremely challenging because the precise identification of the nanometer-wavelength ripples is required [7, 14, 22] and the permeation process is elusive.

Here we report gas permeation through rippled graphene. The feasibility of gas permeation through graphene ripples is determined by detecting the initial oxidation sites of Cu substrate covered with isolated graphene domains. Initial morphological change induced by oxidation of the Cu surface is observed at the Cu areas covered with strongly rippled graphene rather than other areas such as graphene domain boundary. Nudged elastic band (NEB) calculations demonstrate that the oxygen atom permeation occurs via the formation of C–O–C bond, in which process the energy barrier through the rippled graphene lattice is much smaller than that through a flat graphene lattice, rendering permeation through ripples more favorable. Regarding the recent observation on atom intercalation between graphene and metal substrates for transfer-free and electrically insulated graphene [17–19], this discovery not only provides a new insight into the nature of ripple-induced permeation through graphene, reveals the microscopic mechanisms underlying graphene's limited anti-permeation performance, but also highlights the possibility of precisely regulating gas permeation behaviors and electrically decoupling graphene from the metals for graphene nanoelectronics through graphene ripple engineering.

2. Methods

2.1. Graphene synthesis, exposures and transfer

Isolated graphene domains were synthesized on 25 μm-thick polycrystalline oxygen-free Cu foils (Sigma-Aldrich, #349208) at about 1030 °C using methane as the precursor gas (figure S1, supporting information (stacks.iop.org/TDM/4/025010/mmedia)). Different from our previous work [27], here we used oxygen-free Cu foil for the synthesis (figures S2–S4, supporting information). The synthesis was performed using home-made multifunctional integrated graphene synthesis system [27]. Transfer of graphene was accomplished with the assistance of PMMA.

After the synthesis, we cut the samples into several pieces for exposing to different environments. The isolated graphene domain-coated Cu samples were firstly vacuum-sealed in a plastic bag and then were stored in the controlled environments: (1) a desiccator with a relative humidity of 65% and a temperature of 25 °C (designated as 'Air') for 30 d; (2) a desiccator filled with O_2 (pressure of about 0.1 Pa) at room temperature (designated as 'O_2') for 30 d; (3) after the storage in the (2) environment, the sample was immersed into de-ionized water for various time frames at room temperature (designated as 'H_2O'); (4) vacuum-sealed in a plastic bag which was placed an atmospheric laboratory typically with relative humidity of 25% and at 25 °C for various time frames (designated as 'Bag'). These controlled environments allowed us to trace oxidation-induced morphological change (degradation) of the samples, in a manner of either slow or relatively fast process. Note that the sample handling for the storages took about 40 min in a cleanroom (class 1000). Following the exposure, the samples were cut into several pieces further and then loaded into the instrumental chambers for XPS, SHIM, and AES characterizations, which took about 20–40 min in the atmospheric laboratories.

2.2. SEM, AFM, TEM, Raman and XPS

SEM images were obtained on a Hitachi S4800 field-emission SEM system with an accelerating voltage of 3.0 kV. The AFM measurements were carried out on the Veeco Multimode scanning probe microscope in tapping mode. The TEM images and selected area electron diffraction (SAED) patterns were acquired on a FEI Tecnai F20 (field emission gun, 200 kV). Raman spectra (Renishaw, inVia System) of graphene transferred onto 300 nm SiO_2 were obtained with a 532 nm laser (~20 mW power). For XPS characterization (PHI Quantera SXM, ULVAC-PHI) of the graphene-coated Cu samples, monochromatic Al Ka x-ray (operation power of 100 W, 14 × 0.1 mm) with pass energy of 55 eV and a step of 0.1 eV were used. Binding energy corrections for the spectra were carried out using C 1*s* peaks at 284.5 eV as the reference.

2.3. Scanning helium ion microscopy (SHIM)

The SHIM images of graphene-coated Cu surface were obtained using a helium ion microscope (HIM) (Orion Plus, Carl Zeiss). HIM owns a similar mechanism and structure to the field emission scanning electron microscope but uses helium ions instead of electrons as the primary beam. Because all the helium ions are extracted from one atom, the resultant helium ion beam has an ultra-narrow energy distribution, which potentially provides the HIM with a high spatial resolution for secondary electron imaging.

2.4. Scanning Auger electron spectroscopy (AES)

AES measurements were performed at room temperature with a scanning Auger electron spectroscope (ULVAC-PHI model SAM650) with a cylindrical mirror analyzer. The takeoff angle of the instrument was 42°. AES spectra were acquired with a primary electron beam of 10 kV. The incident electron beam current for the AES spectra was about 4.5 nA, as calibrated with a Faraday cup before and after each measurement. Area-analysis mode can be chosen to acquire electron spectra. The acquirement of each elemental map (512 × 512 pixels) took about 3.5 h. The accelerating voltage for sputtering was 1 kV and raster size was 2 mm × 2 mm. The sputtering time used in this work is based on our experience after performing many investigations. We carried out sputtering normally with 0.1 min and 0.3 min intervals.

2.5. Scanning tunneling microscopy (STM)

STM experiments were performed using an *in situ* ultralow-temperature STM system (Unisoku) with a base pressure better than 2×10^{-10} mbar. The samples were heated to about 200 °C in ultrahigh vacuum before being transferred into the STM head. The STM measurements were carried out at 5 K in the constant-current mode with electrochemistry etched W tips. The bias voltage was applied to the sample with respect to the tip. The STM investigated samples were the 'Bag' samples.

2.6. Computational methods

The *ab initio* density functional theory (DFT) calculations were performed using the Quantum-ESPRESSO package. The generalized-gradient approximation (GGA) exchange-correlation functional proposed by Perdew, Burke and Ernzerhof (PBE) was employed. The wave functions and the charge density were expanded with kinetic cutoffs of 40 and 400 Ry, respectively. Electron–ion interactions were described using ultrasoft pseudopotentials. The total energy was converged to within 1×10^{-4} Ry, and the geometry was optimized until the atomic force was less than 1×10^{-3} Ry bohr^{-1}. The reaction pathways for O permeation were calculated using the NEB method with 7 images for each reaction pathway.

3. Results and discussion

By accurately controlling the synthetic conditions [27], isolated rippled graphene [8, 15] domains were synthesized on an oxygen-free Cu substrate (figures 1 and S1–S4, supporting information). The graphene domains conform to the Cu surface, which is characterized by steps and terraces of various sizes (figures 1(a) and (b)). The strong graphene ripples usually formed near the step edges of the Cu substrate [10], as evidenced by scanning tunneling microscopy (STM) topographical images (figures 1(c)–(e) and figure S5, supporting information). The ripples (figure 1(e), red line) had an average amplitude, A, of ~0.08 nm and a period, λ, of ~3.0 nm with a weakly corrugated atomic lattice structure; this pattern is strikingly different from that of the hexagonal lattice taken from the flat terrace (figures S5(a) and (b), supporting information). Weak ripples with relatively smaller amplitudes (~60.0 pm) in graphene appearing as Moiré patterns [28] were also formed on the Cu terrace away from the step edges of Cu substrate (figures S5(c)–(e), supporting information). The individual graphene domains are high-quality with negligible structural defects as confirmed by the local STM visualization (figures 1(c) and (d) and figure S5, supporting information) of the graphene on the Cu substrate and the weak intensity of the D band signal in the Raman spectra acquired from the graphene transferred onto a Si/SiO_2 substrate (figure S6, supporting information). Despite their lobed shape, the graphene domains are single-crystals, as indicated by the uniformly low intensity of the D band [27] and the consistent orientation of the selected area electron diffraction (SAED) spots across the whole graphene domain (figure S7, supporting information).

To investigate the permeation of reactive oxygen species through the rippled graphene, we monitored the oxidation process of the Cu surface covered by the isolated graphene domains after they had been exposed to the controlled environments, i.e. the 'Air', the 'O_2' and the 'H_2O' (see methods and figures S8–S11, supporting information). After the exposure, Cu exhibited oxidation states of 0 (Cu), +1 (Cu_2O) and +2 ($Cu(OH)_2$), as indicated by the Cu_{2p}, Cu_{LMM}, and O_{1s} x-ray photoelectron spectroscopy (XPS) spectra (figure S8, supporting information). The XPS results confirm the oxidation [1, 2] of the Cu coated with rippled graphene.

High-resolution scanning helium ion microscope (SHIM) [29] images (figure 2 and S9–S11, supporting information) of the samples allowed us to observe the morphological alteration incurred by the oxidation, that is, the appearance of bright feature as contrasted by the dark feature of the non-oxidized graphene-covered Cu area (figure 1 and figure S1, supporting information). The morphological alteration was initiated in the vicinity of the Cu step edges, i.e. at the strongly rippled graphene regions, extending along the step edges and gradually expanding onto the terraces (figure 2). The location of morphological alteration at the rippled graphene regions is in good agreement with the recent observation of Cu oxides underneath the graphene nanoripples [30]; however, that report [30] did not investigate why the Cu oxides appeared underneath the graphene nanoripples. In contrast, the graphene domain boundary remained intact and exhibited no morphological change (figures 2(a)–(c) and S9 and S10, supporting information). This could be because of the strong bonding between the graphene domain edge and the Cu substrate [31, 32]. This observation excludes the possibility that the oxidizing agents diffused through the graphene domain boundary to the interface between the graphene and the Cu substrate under the present exposure conditions. Previous studies on the passivation capability of graphene coatings suggested that the presence of domain boundaries and defects in the graphene coatings caused the incomplete passivation, which is attributed to the polycrystalline nature of the continuous graphene coatings that contain numerous graphene domains and domain boundaries [1, 2]. We did observe the morphological changes at the domain boundaries if the samples had been exposed to the 'H_2O' harsh environment for an extended exposure (90 min) (figure S11, supporting information). Furthermore, our observed morphological change shows regular patterns, mimicking the Cu step edges (figures 2 and S9 and S10, supporting information). This rules out the possibility that the observed alteration was caused by negligible defects randomly distributed in graphene domains [2, 33]. To support the

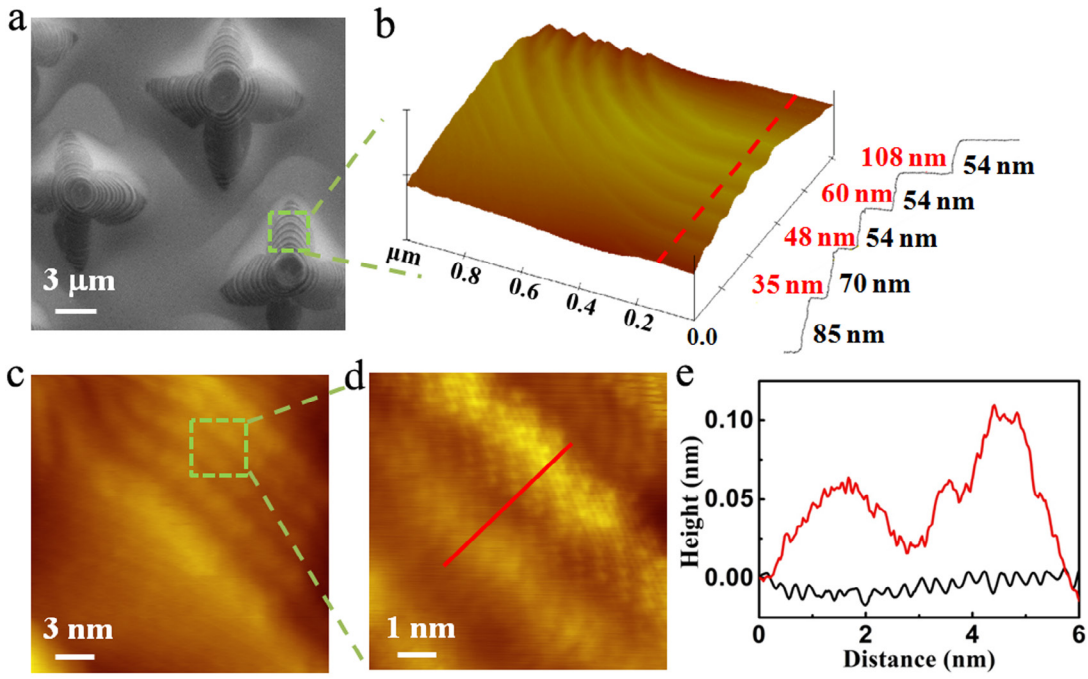

Figure 1. Formation of ripples in graphene domains on the Cu step. (a) SEM image of graphene domains synthesized on Cu substrate. (b) AFM topographical image showing a portion of one branch of the lobed graphene domain, highlighting the steps and terraces. (c) Ultrahigh-vacuum STM topographical images of a graphene domain on the Cu surface acquired at the edge of Cu step (bias: −2.0 V and setpoint: −10.0 pA). (d) Zoomed-in image acquired from the region shown in the dashed square in (c) (bias: −10.0 mV and setpoint: −130.0 pA). (e) Line profile along the red line in (d) as compared to the hexagonal lattice (black line) acquired at the graphene on Cu terrace (figure S5(a), supporting information). The topographical images show corrugations in the graphene adjacent to the edge of Cu step, and the pattern of the lattice structure differs from the hexagonal lattice with a lattice constant of about 0.245 nm of graphene on the Cu terrace.

experimental observation, we calculated the adsorption energy of an oxygen atom at the Cu surface and it is as large as 6.34 eV. This implies that the lateral diffusion probability of oxygen atoms at the Cu surface could be very low and it is easy to form Cu–O bond, i.e. oxidation. Although there were speculations that the morphological change of graphene-covered metals was due to the lateral diffusion of oxidizing agents along the grapheme-metal interface starting at the graphene domain boundaries and defects [34, 35], those previous studies provided no solid evidence of such a proposed diffusion pathway. And if the oxidizing agents diffused through the graphene domain boundaries and defects, the morphological change could appear at the local sites of the domain boundaries (for example, see figure S11, supporting information) and the defects due to the large adsorption energy (6.34 eV) of an oxygen atom at the Cu surface, and then propagate from the local sites to the surrounding areas [36], which is not the case that we observed here. The prominent contrast change within the single-crystal graphene domains reveals the role of graphene ripples in gas permeation through the graphene sheets. Furthermore, no obviously morphological change was observed at the weakly rippled graphene regions localized slightly away from the Cu step edges (figure 2 and S5(c)–(e), supporting information), which indicates that the ratio of the amplitude to period of graphene ripples [25] significantly influenced the permeation (see the supporting information Note 5).

We showed that the distribution of the spatial chemical composition of the rippled graphene-covered Cu, as probed by scanning Auger electron spectroscopy (AES) [27], correlated well with the observed morphological alteration upon oxidation of the underlying Cu (figure 3). The color contrast of the C KLL (figure 3(b)), O KLL (figure 3(c)) and Cu LMM (figure 3(d)) maps within the graphene domains was very sharp, changing with the step edges of the underlying Cu surface. Furthermore, the intensity variation of the O KLL signal was in good agreement with that of the Cu LMM signal, suggesting that oxidation occurred (figures 3(c) and (d)). These findings confirm that the morphological alteration observed in the SHIM images can be ascribed to the oxidation of the Cu surface.

The quantitative intensity changes of the O KLL signal at different areas '2', '3', '4' and '5' (figures 3(e) and (f) and S12, supporting information) were highly consistent with the morphological features. The O KLL signal intensity at area '2' was the strongest, while that at area '5' where there is no surface step, was the weakest. The same intensity change behaviors of the Cu LMM signal and O KLL signal can be ascribed to the occurrence of oxidation, in good agreement with the Auger electron maps. Because of the oxidation, the intensity variation of the C KLL signal showed an opposite trend to that of the O KLL signal, demonstrating that the inhomogeneous C KLL signal distribution within the graphene domains mainly results from oxidation.

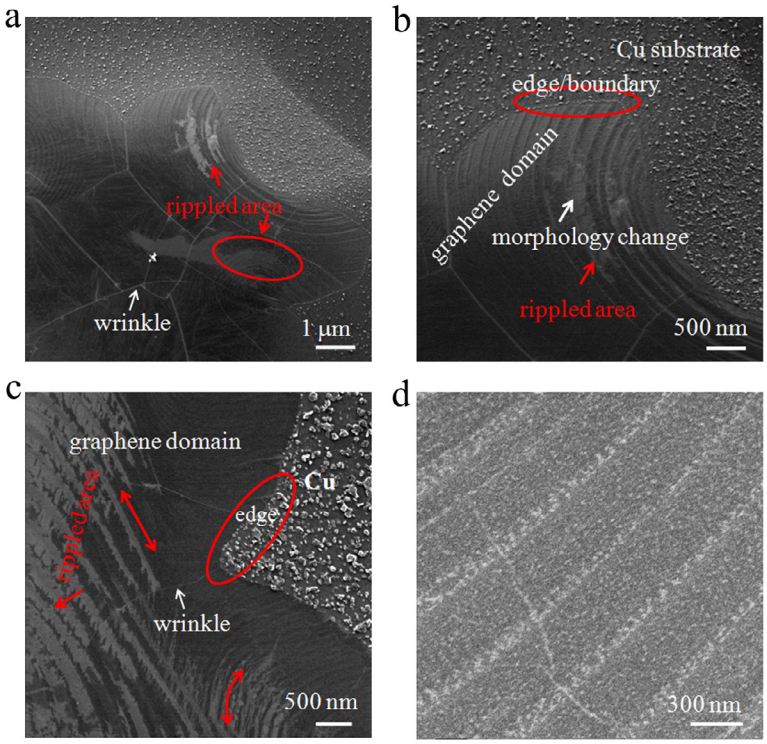

Figure 2. Identification of the morphological changes of the isolated graphene domain-coated Cu samples after the controlled exposures. (a) and (b) The morphological change of a sample after exposed the 'Air'. Morphological change is observed at the rippled graphene area and no change at the graphene domain boundaries/edges as well as the wrinkles. (c) and (d) The morphological change of a sample after exposed the 'H_2O' for 60 min; (d) was acquired at the less degraded area to highlight the regular patterns of morphological change, showing the contrast morphological change near the steps extends along the step and expanded onto the terrace of the underlying Cu. The graphene domain boundary/edge remains intact and morphological change at the wrinkle became appearance.

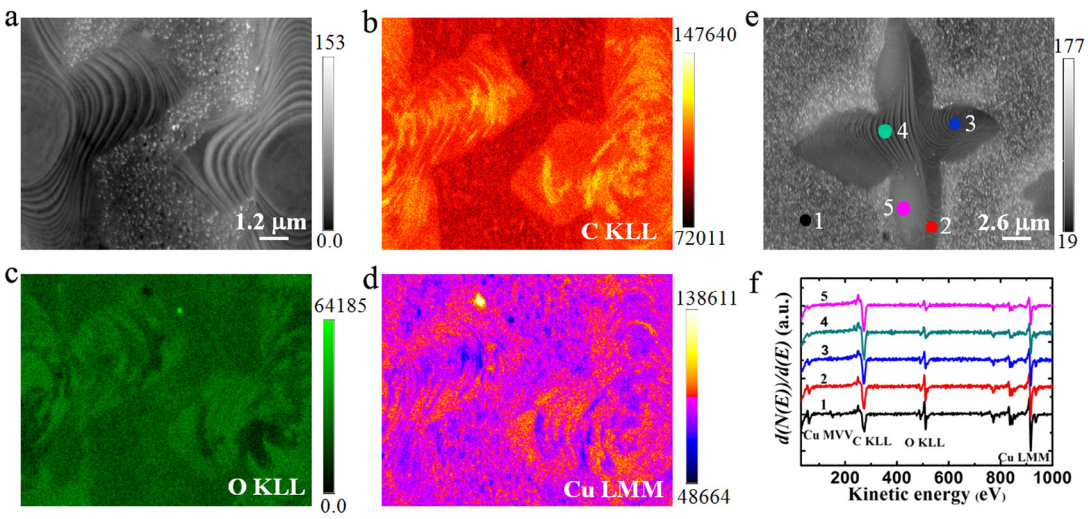

Figure 3. Chemical composition distribution of rippled graphene-coated Cu after exposure to the 'Air' by AES. (a) A secondary electron image of the sample showing the element mapping region. (b) The C KLL Auger electron map. (c) The O KLL Auger electron map. (d) The Cu LMM Auger electron map. These elemental maps show the striking intensity contrast that occurs near the steps of the underlying Cu surface. (e) A secondary electron image showing the areas where the AES spectra were acquired. (f) Differential AES spectra showing all the elements on the surface acquired at the areas marked in (e).

Insights into the permeation mechanisms of oxidative agents, exemplified by the oxygen atom (figure S13, supporting information), through the rippled graphene sheet were gained by *ab initio* density functional theory (DFT) calculations and the climbing-image NEB method [5, 6]. The ripple was modeled with a period-to-amplitude ratio of 11:1. The optimized atomic structure of the ripple initially gave the same C–C bond length as the perfectly flat graphene, indicating that the slight atom wave had no effect on the C–C bond length (figures 4(a) and (b)). We note that the energy barrier calculated for an oxygen atom

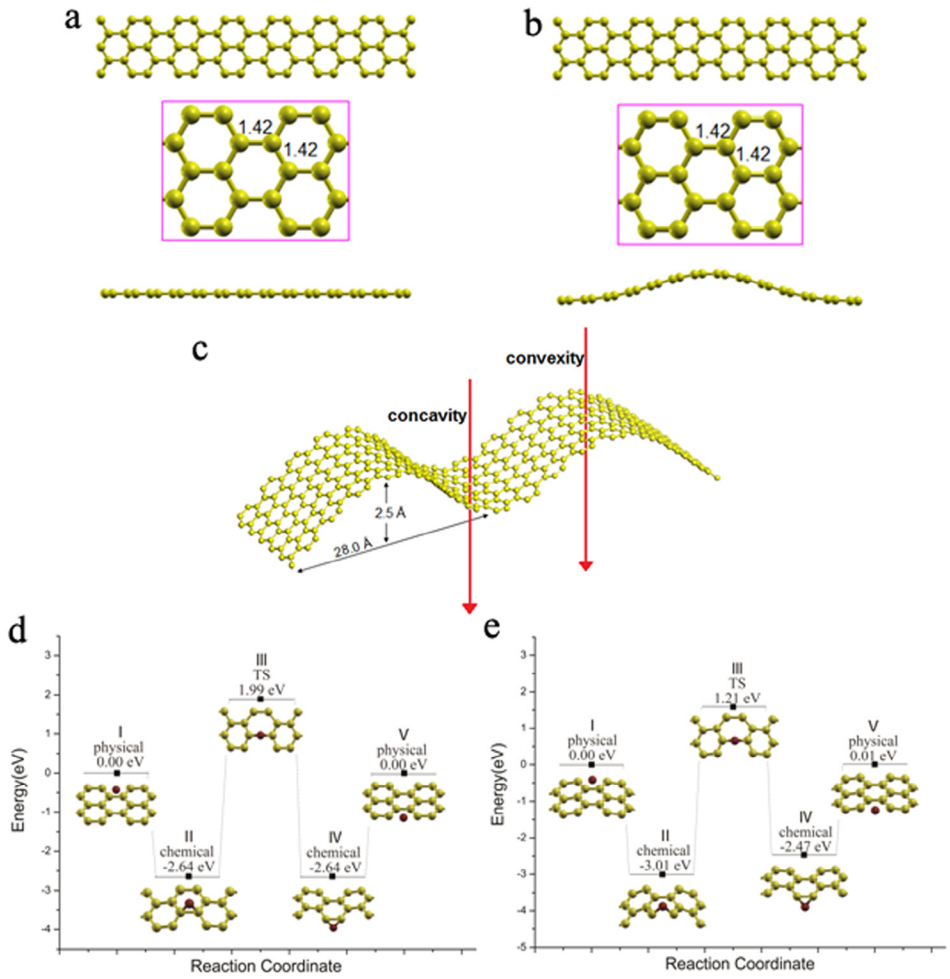

Figure 4. Initial configurations of flat and rippled graphene and NEB calculations of oxygen atom transport through flat and rippled graphene. (a) Flat graphene. (b) Rippled graphene. (c) The sketch map of two routes for oxygen atom transport through rippled graphene. (d) NEB calculations of an oxygen atom passing through flat graphene. (e) NEB calculations of an oxygen atom passing through the rippled graphene with the period-to-amplitude ratio of 11:1. The energy barriers for an oxygen atom to pass through flat graphene and rippled graphene are 1.99 eV (flat graphene, I to II (intermediate state) to III (transition state) in (d)), 1.21 eV (the convex site of rippled graphene, I to II to III in (e)) and 1.20 eV (the concave site of rippled graphene, V to IV (intermediate state) to III in (e)).

passing through graphene ripples is dependent on the amplitude and period of the individual ripples as well as the C–C bond length in the ripples (see the supporting information Note 5).

We had thoroughly searched for the possible pathways by which oxygen atoms resulting from the decomposition of oxygen molecules at Cu surface can permeate through the flat and rippled graphene structures. We found that the oxygen atom most likely broke the C–C bond via the formation of C–O–C bond and passed through the graphene sheet, without existing broken C–C bond after the permeation. Oxygen atoms may permeate through the rippled graphene sheet at both concave and convex sites (figure 4(c)). The NEB calculations (figures 4(d) and (e)) revealed that the energy barriers for an oxygen atom to permeate through the graphene sheets were 1.99 eV (the flat graphene, from I to II to III; figure 4(d)), 1.21 eV (the convex site of the rippled graphene, from I to II to III; figure 4(e)) and 1.20 eV (the concave site of the rippled graphene, from V to IV to III; figure 4(e)). Apparently, the energy barrier for an oxygen atom to pass through rippled graphene was notably lower (0.78 eV and 0.79 eV for the convex and concave sites, respectively) than that for transport through the flat graphene. Therefore, oxygen atoms pass more easily through rippled graphene, at both convex and concave sites, than through flat graphene, with the route through the concave site being the most favorable.

The whole penetration process consists of several sequential steps. First, the oxygen atom chemically adsorbs onto the graphene sheet with the energy reductions of 2.64 eV (figure 4(d), from I to II for flat graphene), 3.01 eV (figure 4(e), from I to II for the convex site of rippled graphene) and 2.48 eV (figure 4(e), from V to IV for the concave site of rippled graphene). In this step, the C–C bond breaks and a C–O–C bond forms. Subsequently, the carbon atoms adjacent to the adsorption site curve out-of-plane towards the oxygen atom, and the corresponding C–C bond stretches simultaneously (figure S13, supporting information), which leads to the permeation of the oxygen atom

through the graphene sheet by overcoming an energy barriers of 4.63 eV for the flat graphene (figure 4(d), from II to III), 4.22 eV for the convex site of the rippled graphene (figure 4(e), from II to III) and 3.68 eV for the concave site of the rippled graphene (figure 4(e), from IV to III). The energy needed for an oxygen atom to permeate through the concave site of the rippled graphene is notably lower than for the flat graphene and the convex site of the rippled graphene (by 0.95 eV and 0.54 eV, respectively).

For a comparison, we also calculated the required energies for an oxygen atom diffusion through the graphene boundary/edge (figure S14, supporting information). The first step is the formation of a C–O–Cu bond, in which the required energy is negligible. The consecutive step is the breaking of the C–O–Cu bond, re-forming of a C–Cu bond, and the oxygen atom entering into the interface between the graphene and the Cu substrate. This step requires overcoming an energy barrier of 3.20 eV. Certainly, this value is much smaller than that of the permeation through the flat graphene sheet (4.63 eV). Secondly, the value is comparable to that (4.22 eV for the convex site and 3.68 eV for the convex site) of the permeation through the graphene ripple with the amplitude-to-period ratio of 1:11. It is worth noting that the energy barrier of the permeation through graphene ripples may be lower or higher, relying on the amplitude-to-period ratio and the C–C bond length of the ripples (see the supporting information Note 5), than that through the graphene domain boundary. The calculations suggest that an oxygen atom can permeate through both the graphene ripples and the graphene domain boundary. Nevertheless, the lateral diffusion probability of oxygen atoms at the Cu substrate is low due to its large adsorption energy at the Cu surface as addressed above. In fact, this is consistent with our experimental observations that in the initial stage of the exposure, the morphological alteration was observed in the vicinity of some Cu steps, i.e. the rippled graphene areas (figures 2 and S9 and S10, supporting information). Along with the exposure in a harsh environment (figure S11, supporting information), morphological change appeared at the graphene domain boundary.

4. Conclusion

In summary, the experimental results and the theoretical studies reveal that gases could permeate through graphene ripples at room temperature due to the lattice curve change in the ripples. This discovery provides new perspectives regarding graphene's limited anti-permeation performance and intercalation mechanisms of different materials into the interface between graphene and its metal substrate, and enables the rational design of graphene-based encapsulation methods for barrier and selective gas separation applications. Moreover, the permeated oxidizing species could alter the interface properties between graphene and the Cu substrate, rendering the electrically isolated graphene for direct applications in graphene optoelectronics.

Acknowledgments

This work was supported by the Program for 14th China–Japan S&T Cooperation (2013DFG52800), the National Natural Science Foundation of China (Grant 51472219, 51672244, 21676232), and the Research Fund for the Doctoral Program of Higher Education (20130101110123). We thank Material Analysis Station at National Institute for Materials Science (NIMS), Japan for the using of AES instrument.

References

[1] Chen S *et al* 2011 *ACS Nano* **5** 1321–7
[2] Wlasny I, Dabrowski P, Rogala M, Kowalczyk P J, Pasternak I, Strupinski W, Baranowski J M and Klusek Z 2013 *Appl. Phys. Lett.* **102** 111601
[3] Bunch J S, Verbridge S S, Alden J S, van der Zande A M, Parpia J M, Craighead H G and McEuen P L 2008 *Nano Lett.* **8** 2458–62
[4] Tsetseris L and Pantelides S T 2014 *Carbon* **67** 58–63
[5] Miao M, Nardelli M B, Wang Q and Liu Y 2013 *Phys. Chem. Chem. Phys.* **15** 16132–7
[6] Hu S *et al* 2014 *Nature* **516** 227–30
[7] Fasolino A, Los J H and Katsnelson M I 2007 *Nat. Mater.* **6** 858–61
[8] Vázquez de Parga A L, Calleja F, Borca B, Passeggi M C G, Hinarejos J J, Guinea F and Miranda R 2008 *Phys. Rev. Lett.* **100** 056807
[9] Shenoy V B, Reddy C D, Ramasubramaniam A and Zhang Y W 2008 *Phys. Rev. Lett.* **101** 245501
[10] Bao W, Miao F, Chen Z, Zhang H, Jang W, Dames C and Lau C N 2009 *Nat. Nanotechnol.* **4** 562–6
[11] Katsnelson M I and Fasolino A 2013 *Acc. Chem. Res.* **46** 97–105
[12] Los J H, Fasolino A and Katsnelson M I 2016 *Phys. Rev. Lett.* **116** 015901
[13] Guinea F, Katsnelson M I and Vozmediano M A H 2008 *Phys. Rev.* B **77** 075422
[14] Tapasztó L, Dumitrică T, Kim S J, Nemes-Incze P, Hwang C and Biró L P 2012 *Nat. Phys.* **8** 739–42
[15] Bai K K, Zhou Y, Zheng H, Meng L, Peng H L, Liu Z F, Nie J C and He L 2014 *Phys. Rev. Lett.* **113** 086102
[16] Pudlak M, Pichugin K N and Nazmitdinov R G 2015 *Phys. Rev.* B **92** 205432
[17] Mao J *et al* 2012 *Appl. Phys. Lett.* **100** 093101
[18] Lizzit S *et al* 2012 *Nano Lett.* **12** 4503–7
[19] Larciprete R *et al* 2012 *ACS Nano* **6** 9551–8
[20] Jiang D, Cooper V R and Dai S 2009 *Nano Lett.* **9** 4019–24
[21] Celebi K, Buchheim J, Wyss R M, Droudian A, Gasser P, Shorubalko I, Kye J I, Lee C and Park H G 2014 *Science* **344** 289–92
[22] Geringer V, Liebmann M, Echtermeyer T, Runte S, Schmidt M, Rückamp R, Lemme M C and Morgenstern M 2009 *Phys. Rev. Lett.* **102** 076102
[23] Katsnelson M I and Geim A K 2008 *Phil. Trans. R. Soc.* **366** 195–204
[24] Gibertini M, Tomadin A, Guinea F, Katsnelson M I and Polini M 2012 *Phys. Rev.* B **85** 201405
[25] Boukhvalov D W and Katsnelson M I 2009 *J. Phys. Chem.* C **113** 14176–8
[26] Wu Q *et al* 2013 *Chem Commun.* **49** 677–9
[27] Liang T, He G, Huang G, Kong Y, Fu W, Chen H, Wang Q, Iwai H, Fujita D, Liu Y and Xu M 2015 *Adv. Mater.* **27** 6404–10

[28] Miranda R and Vázquez de Parga A L 2009 *Nat. Nanotechnol.* **4** 549–50
[29] Guo H, Gao J, Ishida N, Xu M and Fujita D 2014 *Appl. Phys. Lett.* **104** 031607
[30] George L, Gupta A, Shaina P R, Gupta N D and Jaiswal M 2015 *Nanotechnology* **26** 495701
[31] Zhang X, Wang L, Xin J, Yakobson B I and Ding F 2014 *J. Am. Chem. Soc.* **136** 3040–7
[32] Liu L *et al* 2014 *Proc. Natl Acad. Sci.* **111** 16670–5
[33] Weatherup R S, D'Arsié L, Cabrero-Vilatela A, Caneva S, Blume R, Robertson J, Schloegl R and Hofmann S 2015 *J. Am. Chem. Soc.* **137** 14358–66
[34] Yoon T, Mun J H, Cho B J and Kim T-S 2014 *Nanoscale* **6** 151–6
[35] Feng X, Maier S and Salmeron M 2012 *J. Am. Chem. Soc.* **134** 5662–8
[36] Boutilier M S H, Sun C, O'Hern S C, Au H, Hadjiconstantinou N G and Karnik R 2014 *ACS Nano* **8** 841–9